BIBECHANA
Vol. 21, No. 3, December 2024, 195-212

ISSN 2091-0762 (Print), 2382-5340 (Online)
Journal homepage: http://nepjol.info/index.php/BIBECHANA
Publisher: Dept. of Phys., Mahendra Morang A. M. Campus (Tribhuvan University) Biratnagar

Characterization of atmospheric pressure circular dielectric barrier discharge via electrical and optical methods

Roshan Chalise[1,2*], Krishna Regmi[2], Sadip Nepal[2], Sangat Sharma[1], Suresh Basnet[1], and Raju Khanal[1]

[1]*Central Department of Physics, Tribhuvan University, Kirtipur, Kathmandu 44613, Nepal*
[2]*Amrit Campus, Department of Physics, Tribhuvan University, Kathmandu 46600, Nepal*

[*]Corresponding author. Email: plasma.roshan@gmail.com

Abstract

This research work is concerned with the comprehensive study of the electrical and optical characterization of an atmospheric pressure circular dielectric barrier discharge (APCDBD) in natural air. The effect of airflow and input voltage on the power supply's behavior has been investigated to keep the constant electrode gap . The energy and power dissipated during the discharge per cycle are calculated by the Lissajous plot and the time average of the voltage and current curve. For the optical characterization of APCDBD, light emission during the plasma discharge is examined and the electron excitation temperature, rotational temperature, vibrational temperature, and plasma density have been computed. The Boltzmann plot method is used to estimate the electron excitation temperature and vibrational temperature. The rotational and also vibrational temperatures are calculated using online MassiveOES software. It is found that multiple filamentary micro discharge is increased while increasing the airflow and input voltage of the power supply. Energy per cycle of the discharge is increased for increasing input voltage and vice-versa in airflow. The discrepancy in the calculation of energy dissipation from discharge between time-averaged and Lissajous's plot method is estimated. However, the fluctuation is less in the Lissajous's plot method; hence, the energy calculation from the Lissajous plot method is more suitable for plasma discharge. The power consumption of the plasma reactor is found to be dependent on the input of the power supply. Electron excitation temperature and the rotational temperature of the discharge decrease with increasing the airflow in the discharge and increase with increasing input voltage. Therefore, by using the airflow in dielectric barrier discharge, we can move closer to the room temperature of atmospheric pressure plasma.

Keywords
Boltzmann plot, electrical parameters, electron excitation temperature, Lissajous curve, rotational temperature, vibrational temperature.

Article information
Manuscript received: January 19, 2024; Revised: April 19, 2024; Accepted: April 23, 2024
DOI https://doi.org/10.3126/bibechana.v21i3.62034

1 Introduction

In recent years, low-temperature atmospheric pressure plasma has received a lot of attention as it is widely used in diverse fields of science and technology [1–8]. The dielectric barrier discharge (DBD), one of the various forms of atmospheric low-temperature plasma reactors, has a wide range of industrial uses [9, 10]. At atmospheric pressure, the DBD normally operates in a filamentary discharge condition, which restricts the possibilities for its industrial application. However, specific circumstances, homogeneous DBD can be produced, and it has the potential for use in a variety of industrial processes, including plasma sterilization, thin-film deposition, material surface treatment, remediation of diesel-contaminated soil, evaluation of bio-compatibility, and many more [11–15]. In the region of non-thermal plasma where thermal non-equilibrium between the electron, ions, and neutrals exists, the electron temperature can be orders of magnitude higher than the temperature of the heavier particles (atoms, molecules, and ions). These plasma do not heat any surfaces as they come in contact with because the ions and the neutrals stay relatively cool [16]. Due to these properties, it is possible to handle heat-sensitive materials, such as polymers and biological tissues, as well as low-temperature plasma chemistry. The DBD plasma typically consists of a large number of microscopic micro-discharges or filamentary that last for only a nanosecond or microsecond. The uniformity of the DBD is highly desired for industrial applications, particularly for operations involving surface treatment [17]. Due to helium gas has low breakdown voltage and the long lives of the metastable species, it is simple to create homogeneous DBDs, but the process is expensive and inefficient. Since argon and nitrogen are less expensive gases, it is preferable to construct a homogeneous DBD using them [18, 19]. Since argon's mean free path is short at atmospheric pressure, the breakdown voltage is comparatively larger which may make the glow-to-arc transition easier to occur. Because of this, it is challenging to achieve large-gap homogeneous DBD in argon gas between two plane-parallel electrodes [20]. Surface dielectric barrier discharge is considered to be especially promising in aerospace engineering [21, 22], biomedical sciences [23], energy conversion, etc [24]. Electrode materials and shapes affect the discharge modes. Meanwhile, the discharge influences electrode surface [25]. In the air, at atmospheric pressure, Mahoney *et al.* created a dielectric barrier discharge plasma. They were calculated that the power consumption for the reactor operating without gap separation ranged from a few watts to a maximum of about 14 W using voltage/charge Lissajous figures. The obtained emission spectrum was mostly within the second positive system of N_2 $\left(C^3\Pi_u \rightarrow B^3\Pi_g\right)$ and the first negative system of N_2^+ $\left(B^2\sum_u^+ \rightarrow X^2\sum_g^+\right)$ [26]. In atmospheric air, surface dielectric barrier discharge plasma often displays filamentary and diffuse discharges [27]. However, Subedi *et al.* reported that a consistent and uniform DBD discharge was noted between the electrodes, which have a gap of 1 to 3 mm and a 1.5 mm dielectric barrier from argon gas. The gas supply is regulated to a flow rate of 2 liters per minute. High voltage (0 to 20 kV) power supply operating at 10 to 30 kHz frequency produced the discharge, with an electron density of around 10^{16} cm^{-3} and an electron temperature of about 1 eV reported [1]. Compared to filamentary-mode discharges with sinusoidal excitation, it is shown that pulsed excitation over a broad voltage range can generate stable and homogeneous DBD with improved energy efficiency. Furthermore, pulsed-excitation DBD uses less discharge power while producing a higher total transferred charge per voltage cycle. The critical voltage for creating homogeneous DBD can be enhanced with water electrodes, and suppressing instabilities with them is desirable for enhancing stability [28]. Fang *et al.* found that homogeneous discharge exists only under certain conditions. The voltage range for maintaining a stable discharge is found to be wider when the barrier thickness is smaller, the gap distance is shorter and the mesh number is greater [29]. Kogelheide applied a damped sinusoidal voltage waveform with oscillation periods in the microsecond time scale to study a volume and a twinning surface DBD created in various nitrogen-oxygen mixtures at atmospheric pressure. It is discovered that the oxygen concentration in the working gas mixture has a significant impact on the electron density, the lowered electric field, and the dissipated power [12]. Using an in-situ treatment technique, Dhakal *et al.* produced spark dielectric barrier discharge plasma and examined the effects on seed germination and water sterilization. Significant alterations were made to the liquids' physicochemical characteristics by the plasma treatment. Following an 8-minute plasma treatment, the concentrations of H_2O_2, NO_2, and NO_3 were raised to 30, 40, and 100 mgL^{-1}, respectively. *E. Coli* and *S. aureus* were nearly eliminated after 8 minutes of plasma treatment. Moreover, after five minutes of treatment with plasma, coriander seeds germinated more easily [11]. The most fundamental characteristics in gas discharges are electron density and electron temperature, and knowing these factors is crucial for optimizing discharge performance [30]. A plasma's electron density and temperature may be measured using a variety of techniques. The Langmuir probe, microwave interferometer, Laser Thomson Scattering, optical emission, and absorption spectroscopy are

the techniques that are most often utilized. The probe method is cheaper but it disturbs the produced plasma. In atmospheric pressure plasma, discharge produced in a small gap between the electrodes, if any probe is inserted between this discharge the properties of discharge differ or discharge is not formed [31]. Therefore, optical emission spectroscopy (OES) which is non-intrusive and provides abundant information about the plasma species, is a potent method that is frequently employed for plasma diagnosis as an alternative to probe measurement. The temperature, chemical species concentrations, and ionization state of the plasma may all be determined by examining and interpreting its spectra [30, 32]. Recently, using the Boltzmann plot technique and the assumption that the plasma is in a state of local thermodynamic equilibrium, the electron temperature in plasma in the atmospheric pressure range has been measured based on the visible spectrum. In a radio frequency-inductive discharge in the atmospheric pressure range, the existence of the local thermodynamics equilibrium (LTE) condition, which must be met to use the Boltzmann plot technique to determine the electron temperature, has been confirmed [33]. In this work, we have produced the atmospheric pressure circular dielectric barrier discharge (APCDBD) with an airflow system in the stainless electrode characterized by electrical and optical methods. Dielectric barrier discharges (DBDs) and their behavior in a variety of applications are the main subjects of current research on the electrical and optical characterization of atmospheric circular DBDs. It seeks to improve material treatment procedures, comprehend plasma dynamics, and optimize reactor designs. Through the use of DBD plasma, these investigations seek to improve material treatment procedures, comprehend plasma dynamics, and optimize reactor designs.To increase the efficacy and efficiency of DBD systems for uses such as surface modification, plasma cleaning, sterilization, and material treatment, the study examines electron density, ion and current density, mean electron energy, and discharge gap voltage. To explore possible applications, the research also looks at electrical breakdown, plasma production, and single filament behavior in DBDs. literature has been found on using airflow in DBD configuration from natural air to reduce the temperature of discharge and comprehensive study of plasma parameters of plasma discharge like electrical parameters, delivered energy and power, electron excitation temperature, plasma density, and rotational and vibrational temperature of atmospheric pressure discharge for variation airflow and input voltage of power supply. The variation of these plasma parameters can affect treatment process of plasma application, which we have implemented in this work.

2 Methodology

The block diagram of the experimental setup employed in this work is shown in figure 1. The APCDBD device consists of two plane-parallel stainless steel circular metal electrodes of diameter 57.23±0.08 mm and thickness 4.36±0.07 mm, respectively: at lower electrodes are covered by a dielectric layer 2.00 mm thickness and 90.00 mm diameter.

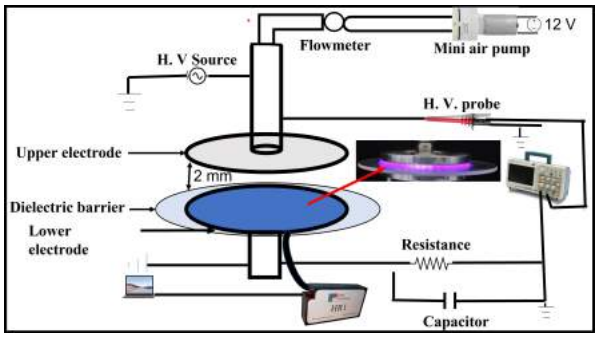

Figure 1: Schematic diagram of APCDBD and its real discharge snapshot.

To ensure stable plasma operation, the gap that separates the electrodes is limited to 4.0 mm wide. Plasma discharge flows in the gap which was produced by a high-voltage power supply (Chengdu Chuangyu Xinjie Technology Co. Ltd.) with an output voltage of 3-30 kV. To control the out voltage of the power supply by changing the input voltage of the power supply (0-24.00 V) DC. The natural airflow is provided on the central hole of the upper electrode by a mini air pump and is regulated by a flow meter. An oscilloscope (Tektronix TBS 1052B) and a 1000 × voltage probe (Pintek HPV -40) were used to measure the voltage across DBD. To monitor the discharge current or transferred charge during plasma formation, a 100 Ω resistor or 10 nf capacitor was connected in series with the ground (10 × voltage probe, Tektronix TPP0201) electrode. The power consumption of discharge was calculated using the Lissajous curve between the applied voltage and the charge produced during the discharge. The method most commonly used for optical characterization is the extraction of the discharge's optical emission spectrum (OES). The light that the discharge emits is detected by an optical emission spectrometer HR1-high-resolution spectrometer (ASEQ Instrument: pixels 3648, signal-to-noise ratio 300:1, exposure time 2.5-600 ms, CCD reading time 14 ms, wavelength 200-820 nm, 10 μm slit, 0.176 nm resolution), 10.0 mm far from the discharge, with 300 ms exposure time and 30 scan average. The APCDBD plasma is generated in different airflow and input applied voltage at fixed electrode gap

and electrode material. Comprehensive electrical parameters such as voltage, current, charge, frequency, energy, and power were calculated as follows: discharge current (I_{dis}) and discharge voltage (V_{dis}) is the corresponding value of current and voltage of the first micro discharge observed in the I-V curve for one complete cycle. Peak-to-peak voltage V_{pp} of the discharge is measured from peak to peak value of the sinusoidal current-voltage waveform. V_{p} of the discharge is half of the peak-to-peak value of the V_{pp} [34];

$$V_p = \frac{V_{pp}}{2} \tag{1}$$

Root mean square (RMS) of sinusoidal voltage in discharge V_{rms} is calculated as [34];

$$V_{rms} = \frac{V_p}{\sqrt{2}} \tag{2}$$

The frequency of the discharge is obtained as the reciprocal of the time of one complete cycle of discharge by [34]

$$\text{Frequency}(f) = \frac{1}{T} \tag{3}$$

We have implemented two ways of calculating of energy and power of the discharge. Five per cycle are carried out to calculate the energy from the voltage-current curve and Lissajous plot, and results are presented per cycle with mean values with standard deviation. The first way is to calculate the time-averaged electrical energy of the plasma discharge using voltage and current curves [34]:

$$E_t = \int V(t) \times I(t) dt \tag{4}$$

where V(t) and I(t) are the voltage and current at the respective time, respectively.
The plasma discharge's time-averaged electrical power consumption can be calculated using [34]

$$P_t = \frac{1}{T} \int V(t) \times V(t) dt = f \times E_t \tag{5}$$

The electrical power calculated by using this method typically fluctuates from cycle to cycle. After that, several cycles are required to get a converged mean value. In addition, to ensure that the current peaks are correctly recorded and provided, the data must be captured using a high sampling rate (usually a few ns) and a high bandwidth oscilloscope. There is still a problem with this approach, despite its relative simplicity and accuracy: when there are strong current peaks, it can be difficult to resolve the synchronous current accurately because its amplitude is at least one order of magnitude smaller than the current peaks [35]. To overcome this issue Manley et al. (1943) developed another simple method [36] used for surface DBD plasma [37]. This method consists of placing a capacitor C between the grounded electrode and the earthing point as shown in figure 1. It is accomplished by plotting the charge curve of the inserted 10 nf capacitor throughout a full cycle as a function of the applied voltage. Each period's energy dissipated by the discharge is represented by the area inside the closed Lissajous curve. The shape of the Lissajous curve depends on various factors, including the frequency, amplitude, and phase relationship between the two waveforms. So, to obtain the area of the Lissajous curve, the applied voltage and the charge accumulated curve are plotted. If we take one full cycle of discharge data, the area of this curve indicates the energy that the discharge releases for each cycle [36]. The energy dissipated per cycle is calculated by [36]

$$E_L = \text{Area covered by Lissajous (Q-V) plot} \tag{6}$$

Using the Lissajous (Q–V plot) approach, the power dissipation across the APCDBD is calculated by multiplying energy with the current-voltage waveform frequency [36]:

$$P_L = (E \times f) \tag{7}$$

This approach's primary benefit is that it is more reproducible from cycle to cycle and does not suffer from bias caused by high current peaks in the computation. Using this method, calculating the precise amount of electrical power utilized only requires one AC cycle. This makes sense for tests conducted in closed loops where a short loop time is required [35]. The energy and power calculation from every four full cycles of the I-V curve and presented in mean and standard deviation.
Optical spectroscopy is a widely used technique to measure the intensity of different wavelengths of light. Because they are noninvasive and have a fast response time, spectroscopic diagnostics are useful for measuring plasma temperatures, density, and several other characteristics in plasma that can be computed with the help of optical spectroscopy. The optical emission spectra are taken ten times and presented as their mean. The plasma temperatures are categorized into four types, i.e., the electron, vibrational, rotational, and translational temperatures [38]. Since there is a high frequency of energy exchange between the rotational and translational temperatures of the plasma, they are thought to be nearly equal [38, 39]. However, the rotational temperature T_{rot} is typically referred to as the temperature of the kinetic gas [38]. Understanding vibrational temperature T_{vib} can help one understand the relative rates of energy exchange processes between vibration and translation [40] and is an important factor in understanding the synthesis of

NO_2 and the quenching of O_3 [41]. Plasma's vibrational and rotational temperatures are crucial factors that can impact both the target material's surface properties and the rate at which the plasma is chemically reacting. Higher vibrational temperatures have the potential to significantly accelerate chemical reactions in plasma because they indicate the presence of energy in the excited state of molecular vibration. Rotational temperature describes the population of rotational levels in molecular organisms [42].

In plasma physics, electron temperature (T_e) is one of the most fundamental and instructive characteristics since electrons control the chemical reactions occurring within the plasma in addition to being involved in the excitation, dissociation, and ionization of atoms and molecules. Since excitation mechanisms that control the distribution of excited states are primarily driven by free electrons, the kinetic temperature of the free electrons is typically correlated with the T_{exc} of the bound electrons in an atom or molecule [43]. In high-pressure plasmas, excitation temperature is commonly used. In particular, because of their close association, determining T_e at atmospheric pressure often depends on T_{exc} measurement. T_{exc} is near T_e if the system abides by the local thermodynamic equilibrium (LTE). Thus, measuring T_{exc} can be a useful substitute diagnostic for plasma discharge [43, 44]. Numerous diagnostic methods are available for determining the electron temperature of the plasma; however, the electrostatic Langmuir probe is one of the most widely used and flexible technologies for this purpose [45]. Despite having a straightforward hardware setup, its application may be restricted at times because of issues with analysis, particularly when negative ions are present, a potential source of plasma disruption, and difficulties using it with large-volume plasmas. T_{exc} can also be ascertained using optical emission spectroscopy using the proper equilibrium models [44].

The Boltzmann plot method is one of the most widely used techniques for measuring the temperature in lab plasmas. The radiative transfer equation for an optically thin, uniform, and isothermal plasma along the line of sight provides the basis for this calculation. The equation is linearized by taking the logarithm of both portions to get the Boltzmann plot. The argument of the logarithm, a dimensionless transcendental function, must also be dimensionless [46]. The Boltzmann plot technique of N(III) species, which uses the data from the NIST database [47] in table 1, is used to compute the electron excitation temperature (T_{exc}). Using this approach, the LTE plasma equation is [48];

$$\ln\left(\frac{\lambda_{ij}I_{ij}}{A_{ij}g_j}\right) = -\frac{E_j}{k_B T_{exc}} + K \tag{8}$$

The variables in equation (8) are the intensity of the transition from the i to the j state (I_{ij}), wavelength of the transition (λ_{ij}), transition probability (A_{ij}), statistical weight (g_j), higher energy level E_j, electron excitation temperature T_{exc}, and constant K. When we plot the $\ln\left(\frac{\lambda_{ij}I_{ij}}{A_{ij}g_j}\right)$ versus E_j, the slope of the obtained graph (Boltzmann plot) is equal to -$\frac{1}{k_B T_{exc}}$ and then the electron excitation temperature is obtained.

Table 1: Selected N(III) peaks in optical emission spectroscopy of APCDBD and its corresponding spectroscopic data [47] for plotting of Boltzmann plot.

λ_{ij} (nm)	A_{ij} (s^{-1})	E_j (eV)	g_i-g_j
336.734	1.27×10^8	39.35199	6–6
375.467	3.78×10^7	38.95798	4–6
377.105	5.59×10^7	38.95798	4–4
393.852	8.96×10^7	41.48118	4–6
399.863	1.76×10^8	42.49548	4–6
400.358	1.88×10^8	42.49560	6–8

The Saha equation is rooted in the principles of statistical mechanics and considers the balance between ionization and recombination processes in plasma at thermal equilibrium. It provides a way to calculate the relative abundances of different ionization states of an element in plasma as a function of temperature and pressure. The plasma density is calculated from the Saha-Boltzmann equation [49]:

$$N_e = 2\frac{I_2 A_1 g_1 \lambda_2}{I_1 A_2 g_2 \lambda_1}\left(\frac{2\pi m_e k_B T_{exc}}{h^2}\right)^{3/2} \exp\left[-\frac{(E_1 - E_2 + E_j)}{k_B T_{exc}}\right] \tag{9}$$

The energy of ionization of a neutral atom is denoted by E_j; the intensity of the same species line has a larger gap in upper energy, and the wavelengths are denoted by λ_1 and λ_2; the transition probabilities are represented by A_1 and A_2; and the statistical weights are g_1, g_2.

Rotational (T_{rot}) and vibrational (T_{vib}) temperatures are calculated by MassiveOES software [50–52], in which measured OES spectrum is fitted with the standard spectrum and provide the results with residual error in fitting both spectra. When dealing with nitrogen plasmas or plasmas containing nitrogen, Boltzmann plots or fits of the band envelopes of various bands belonging to the first negative system and/or second positive system are commonly employed [53]. So the vibrational temperature is calculated by the Boltzmann plot method also. The line intensity of the vibrational transition's spectral was provided as [54]

$$I_{\nu'\to\nu''} \propto \frac{hc}{\lambda_{\nu'\to\nu''}} A_{\nu'\to\nu''} N_0 \exp\left(-\frac{hcG_{\nu'}}{k_B T_{vib}}\right) \tag{10}$$

where k_B, h, c, and T_{vib} are the Boltzmann constant, velocity of light, and vibrational temperature respectively, I, A, G, and λ are transition frequency, Einstein coefficient and spectral term of vibrational transition and wavelength which are related to upper vibrational level (ν') to lower vibrational level (ν"). The spectral factor can be replaced by the energy difference of the energy levels $G'_\nu = E_{\nu'} - E_0$. The vibrational energy of the excited molecules on the level of N_2 ($C^3\Pi$) in the quantum harmonic oscillator approximation disregarding the anharmonicity constant [55];

$$E_\nu(eV) = 1.2398 \times 10^{-4}(\nu + \frac{1}{2})w_e(\mathrm{cm}^{-1}) \quad (11)$$

where ν is the vibrational quantum number, which can be 0, 1, 2, 3,... of ground level, and w_e is the spacing of vibrational energy on the $C^3\Pi$ (= -2047.17 cm^{-1}). After applying eq. (11) in eq. (10) then we can get the semi-log equation as

$$\ln\left(\frac{I_{\nu'\to\nu''}\lambda_{\nu'\to\nu''}}{A_{\nu'\to\nu''}}\right) = C - \frac{E_{\nu'} - E_0}{k_B T_{vib}} \quad (12)$$

where $I_{\nu'\to\nu"}$ is the intensity of transition from upper to lower state, $\lambda_{\nu'\to\nu''}$ is the wavelength of transition, $A_{\nu'\to\nu''}$ is the transition probability, $E_{\nu'}$ is the upper energy level with the vibrational quantum numbers. When we plot the $\ln\left(\frac{I_{\nu'\to\nu''}\lambda_{\nu'\to\nu''}}{A_{\nu'\to\nu''}}\right)$ versus $(E_{\nu'} - E_0)$, the slope of the obtained graph (Boltzmann plot) is equal to $-\frac{1}{k_B T_{vib}}$ and then the vibrational temperature is obtained. N_2 species have a high vibrational temperature, which is shown by the overpopulation of N_2 vibrational states. For the Boltzmann plot method, four vibrational bands are taken: $\Delta\nu$= +1 (1-0, 2-1), $\Delta\nu$= -1 (0-1, 1-2, 2-3), $\Delta\nu$= -2 (0-2, 1-3, 2-4) and $\Delta\nu$= +2 (2-0, 3-1) [56]. The National Institute of Standards and Technology reference database is the source of the spectroscopic parameters needed for the Boltzmann plot [47]. The parameters to obtain the vibrational temperature is based on the analysis of the N_2 ($C^3\Pi$) or the second positive system emissions of $\Delta\nu = \nu'$-ν'', vibrational transition (ν''-ν') [56], wavelength λ (nm) [55], transition probability $A\nu' \to \nu''$ (10^6 s^{-1}) [55] and energy $E_{\nu'}$ (eV) calculated according to eq. (11) are listed in table 2.

Table 2: Selected wavelengths of the OES spectrum and all other parameters required to Boltzmann plot of T_{vib} [55].

$\Delta\nu$	(ν''-ν')	λ (nm)	$A\nu' \to \nu''$ (10^6 s^{-1})	$E_{\nu'}$ (eV)
-2	2-4	295.32	3.80	1.14
-2	1-3	296.20	4.62	0.88
-2	0-2	297.68	3.34	0.63
-1	2-3	311.67	1.65	0.88
-1	1-2	313.60	5.49	0.63
-1	0-1	315.90	8.88	0.38
0	0-0	337.10	13.90	0.12
+1	2-1	353.60	11.41	0.38
+1	1-0	357.69	13.80	0.13
+2	3-1	375.54	8.68	0.38
+2	2-0	380.49	4.81	0.13

3 Results and Discussion

The relationship between the applied voltage and the resulting current is an important aspect of DBD plasma. Initially, at low voltages, there's little current flow due to the insulating properties of the dielectric barrier. As the applied voltage increases, the voltage across the gap exceeds the dielectric breakdown voltage, leading to the initiation of plasma discharge and a sudden increase in current [57]. The voltage fault and impulse current occur when the voltage is high enough to ionize the working gas (atmospheric air). When the applied voltage exceeds the breakdown voltage of the atmospheric air, then the micro discharge can be seen [58].

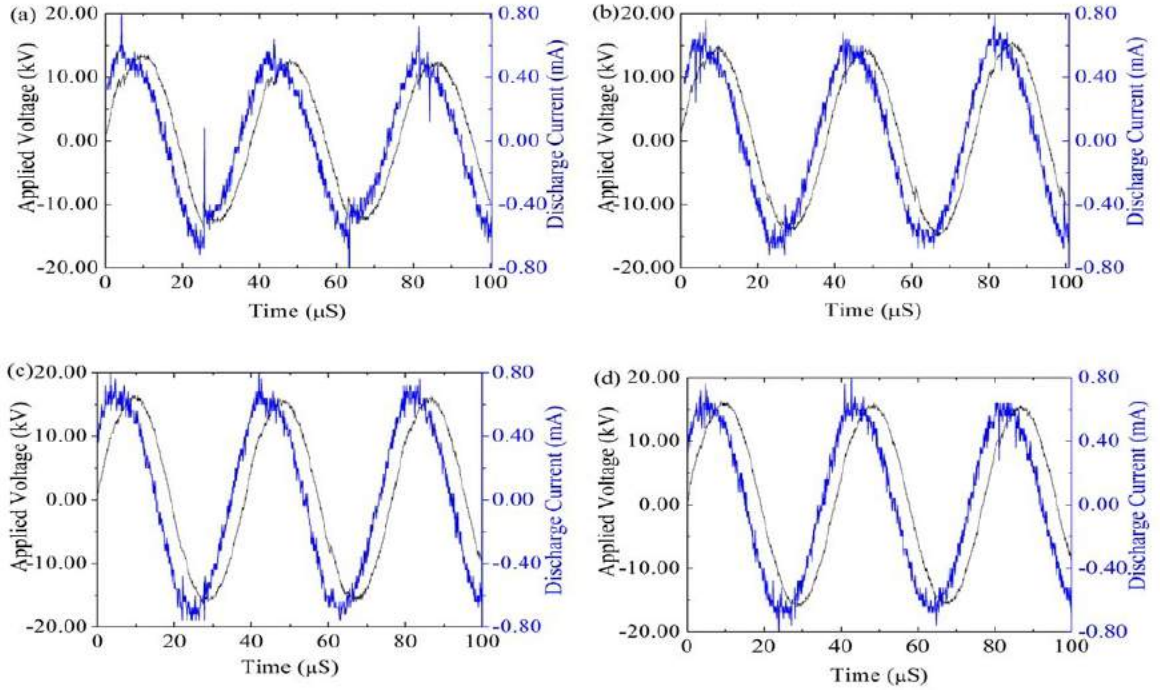

Figure 2: Time variation with voltage and current for the flow variation of (a) 0 LPM, (b) 5 LPM, (c) 10 LPM, and (d) 15 LPM respectively.

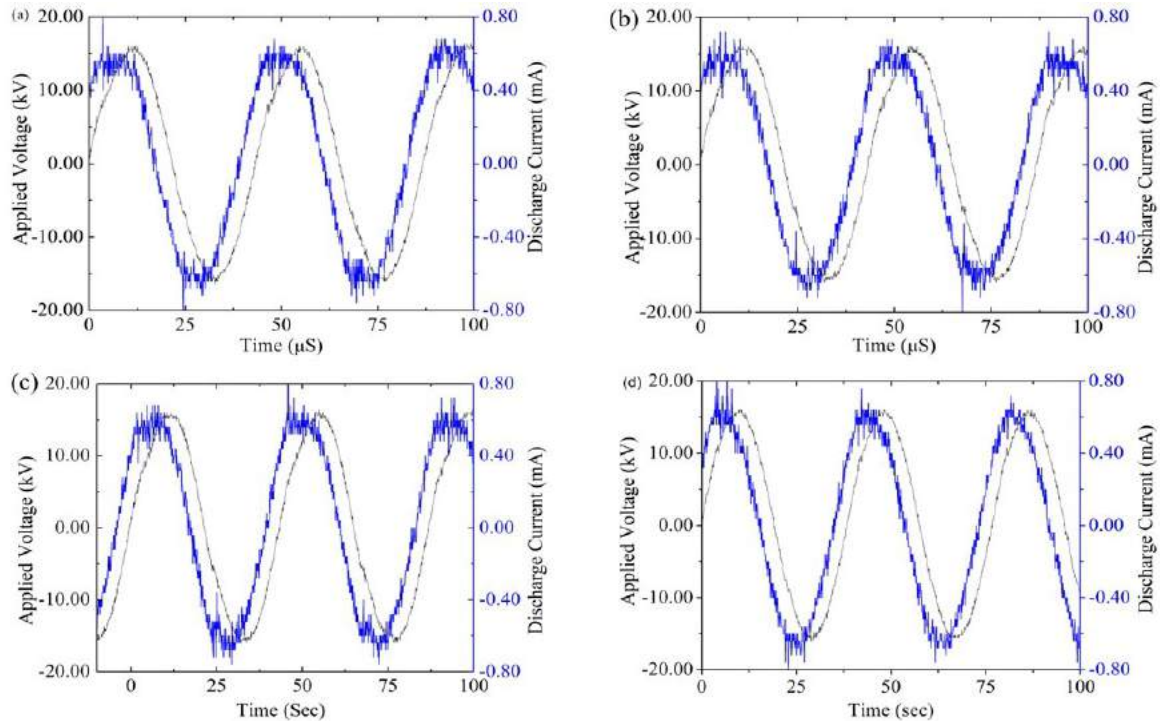

Figure 3: Time variation with voltage and current for the voltage variation of (a) 12.00 V, (b) 16.00 V, (c) 20.00 V, and (d) 24.00 V respectively.

Figure 2 and 3 shows the plot of the discharge current and applied voltage (I-V) waveform at the flow variation at constant input voltage and variation of input voltage at constant air flow rate. The number of current pulses rises and the discharge current intensity falls as flow rates increase from 0 to 15 LPM [59, 60]. The breakdown voltage is also reduced because, when airflow is introduced

into the discharge region, the breakdown moment gradually shifts towards the lower time values. The breakdown voltage drops as airflow enters the discharge space. Consequently, the number of filaments rises while the intensity of the discharge current falls [61]. Because of the lower breakdown voltage, more filaments with lower intensities at a fixed input power can be produced in the discharge region [62].

Figure 4 (a) and (b) represent the Lissajous curve of the different LPM at constant voltage and the varying voltages with constant airflow. It is observed that with increasing the input voltage and airflow, multiple micro discharges are increased in the I-V plot. So that more and more filamentary discharge is observed during the discharge region. The increase in input voltage has resulted in an increase in peak-to-peak voltages and RMS voltage. The energy carried by discharge has also decreased increasing the airflow. The frequency of the discharge is independent of applied airflow. It can be seen that the power delivered by the APCDBD also decreased with an increasing the airflow as shown in the table 3. The increase in input voltage has increased the frequency. The energy and power of the APCDBD plasma increase with increasing the voltage that is shown in table 4. There is the fluctuation of energy from time-averaged and the Lissajous plot method. Up to 10 % fluctuation in airflow and 2 % fluctuation in input voltage. Due to the fewer number of cycles measured from our oscilloscope, more fluctuation of energy occurred, these limitations result in agreement with previous results [35]. However, the fluctuation of energy per cycle is 4 % in airflow variation and less than 1 % in input voltage variation, when calculated from Lissajous plot methods.

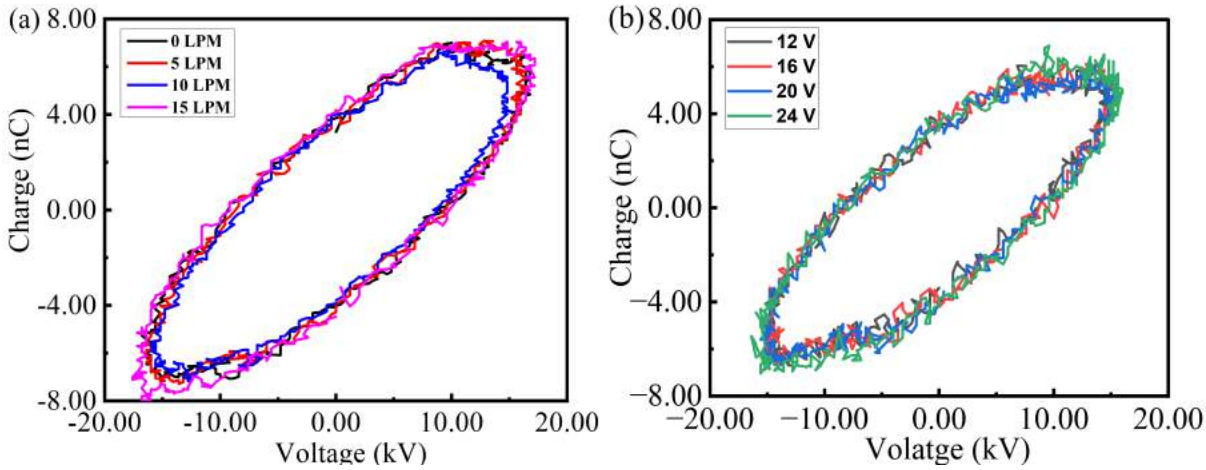

Figure 4: Lissajous plot; charge (Q) concerning the applied voltage (kV) across discharge electrode for different (a) airflow at 24.00 V input voltage, and (b) input voltage at 15 LPM airflow.

Table 3: Electrical parameters of APCDBD for various air flows at 24.00 V input voltage.

LPM	V_{PP} (kV)	V_{rms} (kV)	I_{dis} (mA)	V_{dis} (kV)	E_t (μJ)	E_L (μJ)	f (kHz)	P_t (W)	P_L (W)
0	24.45	8.64	0.41	8.44	116.12±11.98	190.02±1.44	25.60	2.97±0.11	4.86±0.14
5	28.77	10.17	0.75	13.97	158.13±17.01	191.26±7.96	26.10	4.12±0.17	4.98±0.79
10	30.91	10.93	0.87	16.38	160.23±9.68	193.41±6.65	26.70	4.16±0.96	5.02±0.66
15	31.21	11.03	0.88	16.40	179.00±5.35	197.70±4.93	26.90	4.68±0.54	5.15±0.49

Table 4: Electrical parameters of APCDBD at different input voltage at 15 LPM airflow.

V_{in} (V)	V_{PP} (kV)	V_{rms} (kV)	I_{dis} (mA)	V_{dis} (kV)	E_t (μJ)	E_L (μJ)	f (kHz)	P_t (W)	P_L (W)
12.00	30.87	10.91	0.63	5.98	172.99±4.98	156.52±2.57	22.17	3.83±0.11	3.47±0.05
16.00	32.58	11.52	0.68	7.60	172.01±3.22	162.48±3.12	22.98	3.95±0.07	3.73±0.07
20.00	33.03	11.67	0.76	8.70	176.17±4.40	174.96±5.78	24.15	4.25±0.11	4.23±0.13
24.00	33.55	11.86	0.91	9.26	165.63±8.35	186.76±9.39	25.77	4.26±0.21	4.99±0.49

When comparing this power estimating process to the time-averaged integration of the voltage and current over five AC cycles, the deviation of value per cycle is far more up to 10 % by calculating the averaged method and nominal standard deviation found in the Lissajous plot method was used.

3.1 Optical Characteristics

Optical emission spectroscopy (OES) of plasma involves studying the emission of light produced during the plasma discharge and transferring these emission spectra into their wavelength and intensity values. This can provide valuable information about the plasma's properties, such as its composition, temperature, and density. The excitation temperature, plasma density, rotational, and vibrational temperature of the APCDBD are presented here. Figure 5 (a) and (b) show the OES of APCDBD plasma at different air flows and different input voltages. In our research, we have used natural air as a working gas. The intensity of the spectra decreased with increasing the airflow and increased with increasing applied voltage in the power supply observed in the blowup figure of spectra of figure 5 (b). The population of excited particles, which can be produced by one or more channels depending on the plasma conditions, is shown by the emission intensity. The intensity of the electrode field increases in the discharge zone as the applied voltage increases. More energetic electrons are produced in the discharge zone as the electrode field strength increases. After that, they accelerate radiation transitions' higher states, producing more active particles. As a result, when the applied voltage rises, so do the intensities of the corresponding emission spectra [42]. In atmospheric air, there is approximately 78 % of nitrogen and 20 % oxygen. Thus, the peak of OES spectra in APCDBD plasma has almost nitrogen and oxygen species. The major observed spectra are the second positive system (310-380 nm) of N_2 $\left(C^3\Pi_u \rightarrow B^3\Pi_g\right)$ and the first negative system (390-440 nm) of N_2^+ $\left(B^2\sum_u^+ \rightarrow X^2\sum_g^+\right)$ [56]. Additionally, OH $\left(A^2\sum^+ \rightarrow X^2\Pi\right)$ radicals is prominently seen at 309 nm in the spectrum of the gliding arc discharge which plays a crucial role in plasma chemical reactions such as the oxidation of gas and liquid pollutants. The nitric oxide gamma band NO_γ $\left(A^2\sum^+ \rightarrow X^2\Pi\right)$ is observed in 200 to 280 nm. Reactive oxygen (O) radicals are found at wavelengths 777 nm with electronic transitions 4s(3D)4d→4p(3P) [6, 36].

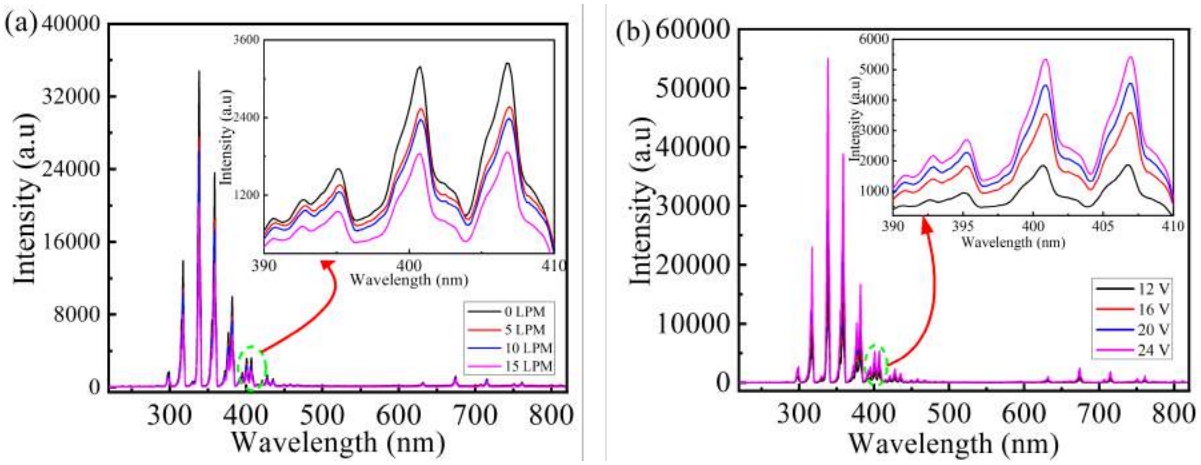

Figure 5: Optical emission spectroscopy and blow-up spectra of APCDBD for (a) various airflow at 24.00 V input, and (b) various input voltage at 15 LPM airflow.

Boltzmann's plot is used to study the electron excitation temperature of the plasma. The energy level of N (III) species of respective wavelength versus relative intensity distribution was plotted to find the electron excitation temperature of APCDBD. A Boltzmann plot is a graphical representation used in spectroscopy to analyze the populations of energy levels within a system. In the context of DBD plasma, which is a type of low-temperature plasma, a Boltzmann plot can be used to understand the energy distribution of excited states of atoms or molecules in the plasma [63]. The slope of Boltzmann's plot of airflow and input voltage variation gives the value of electron excitation temperature as shown in figure 6 and 7 respectively.

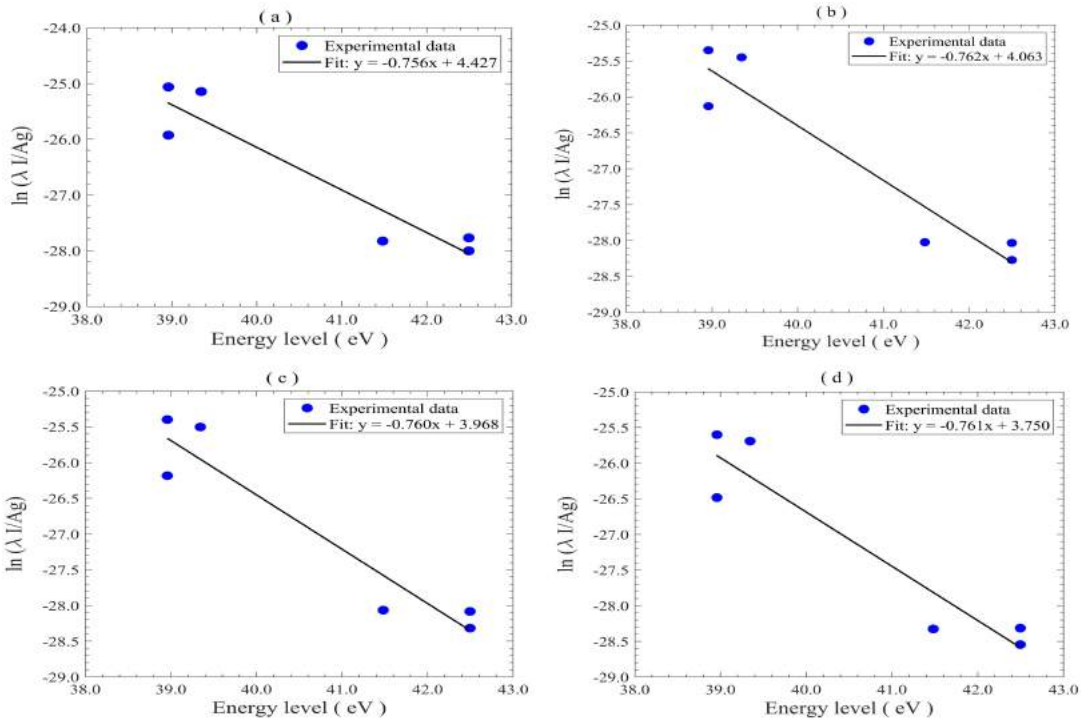

Figure 6: Boltzmann plot for the estimation of T_{exc} using N (III) species for increasing flow variation of (a) 0 LPM, (b) 5 LPM, (c) 10 LPM, and (d) 15 LPM.

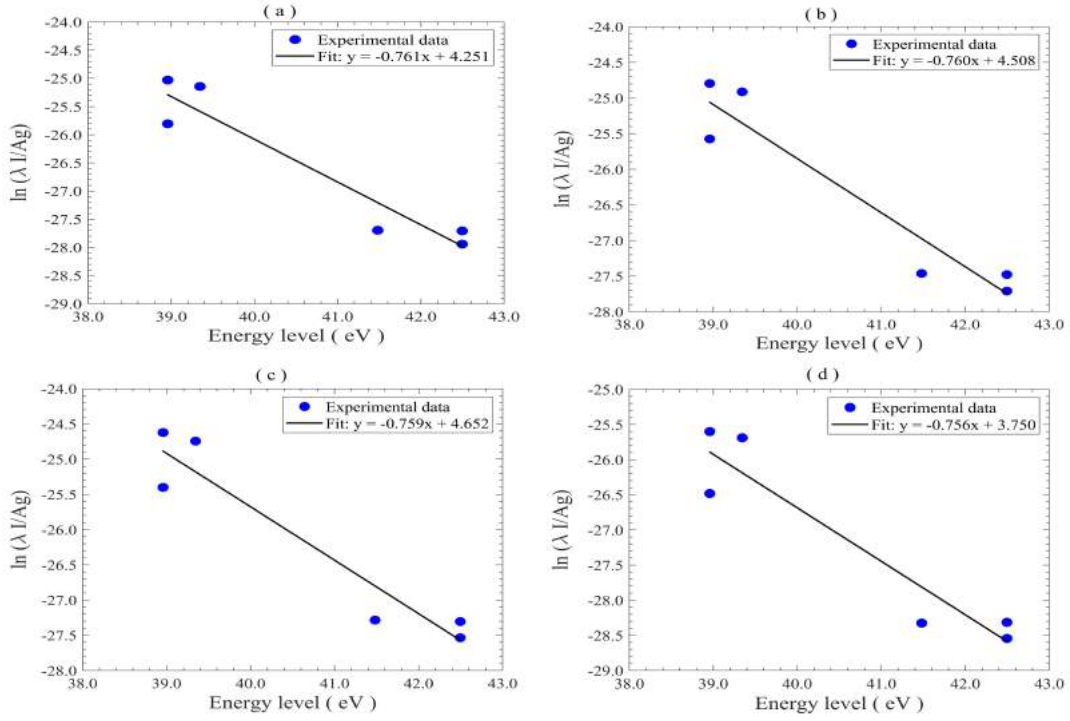

Figure 7: Boltzmann plot for the determination of T_{exc} using N(III) species for increasing applied voltage (a) 12.00 V, (b) 16.00 V, (c) 20.00 V and (d) 24.00 V.

Figure 8 and 9 represent the measured and simulated OES data fitted plot for the determination of T_{rot} and T_{vib} by using nitrogen second positive system N_2 ($C^3\Pi_u - B^3\Pi_g$) from MassiveOES software for increasing flow variation for 0 LPM, 5 LPM, 10 LPM, and 15 LPM and increasing applied voltage at 12.00 V, 16.00 V, 20.00 V, and 24.00 V respectively.

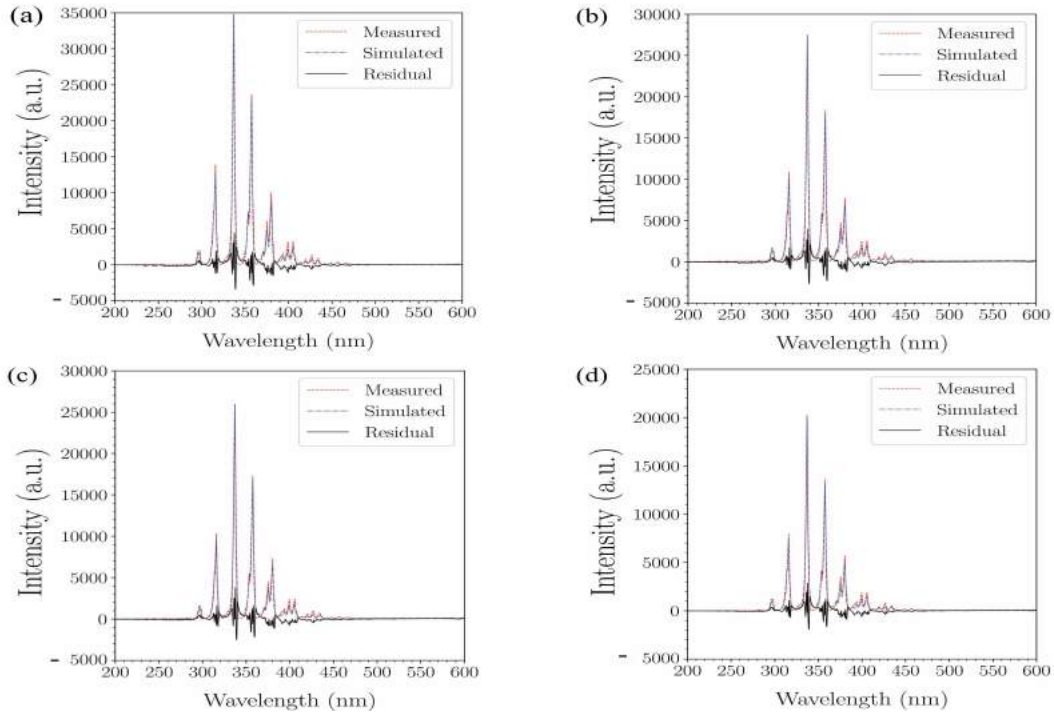

Figure 8: Measured and simulated OES data fitted plot for the determination of T_{rot} and T_{vib} by using nitrogen second positive system (SPS) N_2 ($C^3\Pi_u - B^3\Pi_g$) from MassiveOES software for increasing flow variation for (a) 0 LPM, (b) 5 LPM, (c) 10 LPM and (d) 15 LPM.

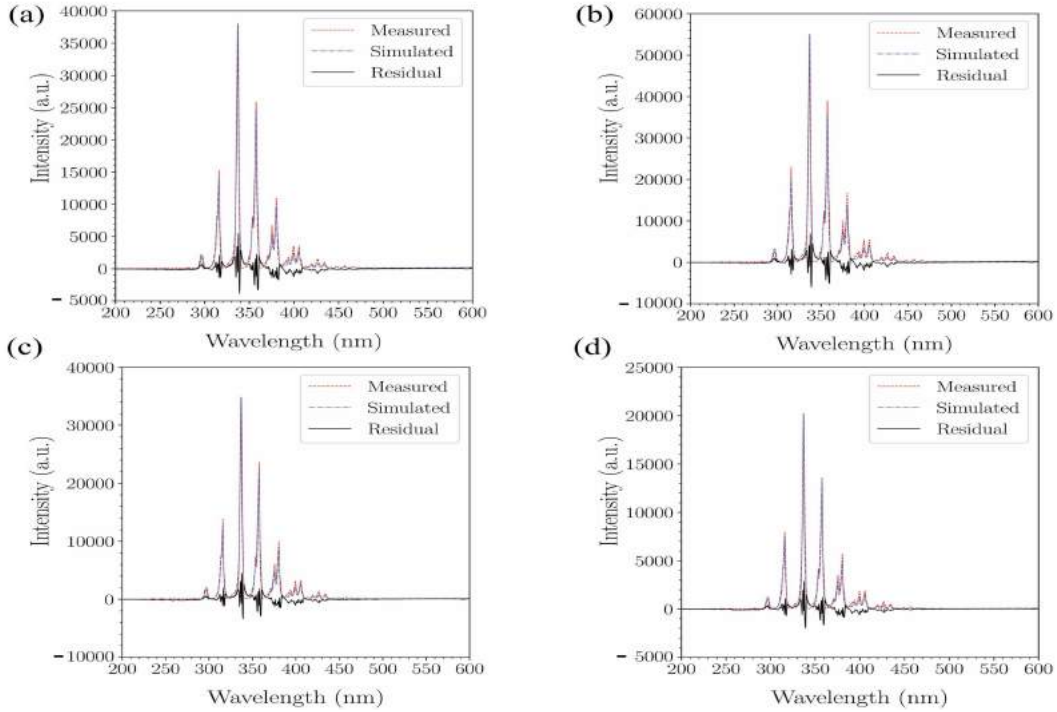

Figure 9: Measured and simulated OES data fitted plot for the determination of T_{rot} and T_{vib} by using nitrogen second positive system N_2 ($C^3\Pi_u - B^3\Pi_g$) from MassiveOES for increasing applied voltage (a) 12.00 V, (b) 16.00 V, (c) 20.00 V and (d) 24.00 V.

T_{rot} is typically utilized as an approximation of the gas temperature (T_{g}) since it is representative of the rotating population of the ground state and provides information on the global temperature of the plasma [64]. The average kinetic energy brought on by the rotating of particles in the plasma is referred to as rotational temperature. The molecular axes of plasma molecules can spin. The energy distribution between these rotating degrees of freedom is shown by the rotational temperature [65]. On the other hand, electron collisions are the primary source of molecular specie's vibrational states. The non-equilibrium plasma's chemical kinetics are significantly influenced by the vibrationally excited species, [66] because vibrational excitation plays the role of an energy reservoir [67]. Figure 10 shows the typical Boltzmann plot of the relative intensity distributions versus vibrational energy using nitrogen second positive system N_2 ($C^3\Pi_u - B^3\Pi_g$) for flow variation of 0 LPM, 5 LPM, 10 LPM, and 15 LPM. The vibrational temperature is correlated with the average kinetic energy of the oscillating motion of the plasma's particle constituents. Atoms and molecules can oscillate about their equilibrium locations as well as other sorts of vibrations that can occur in plasma. The quantity of energy involved in these oscillations is described by temperature variations Figure 10 and 11 shows a typical Boltzmann plot of the relative intensity distributions flow variation and input voltage variation. After taking into account the scattered data points and fitting errors, the vibrational temperature was obtained Figure 11 shows the Boltzmann plot for the determination of T_{vib} using nitrogen second positive system N_2 ($C^3\Pi_u - B^3\Pi_g$) for increasing applied voltage of 12.00 V, 16.00 V, 20.00 V, and 24.00 V.

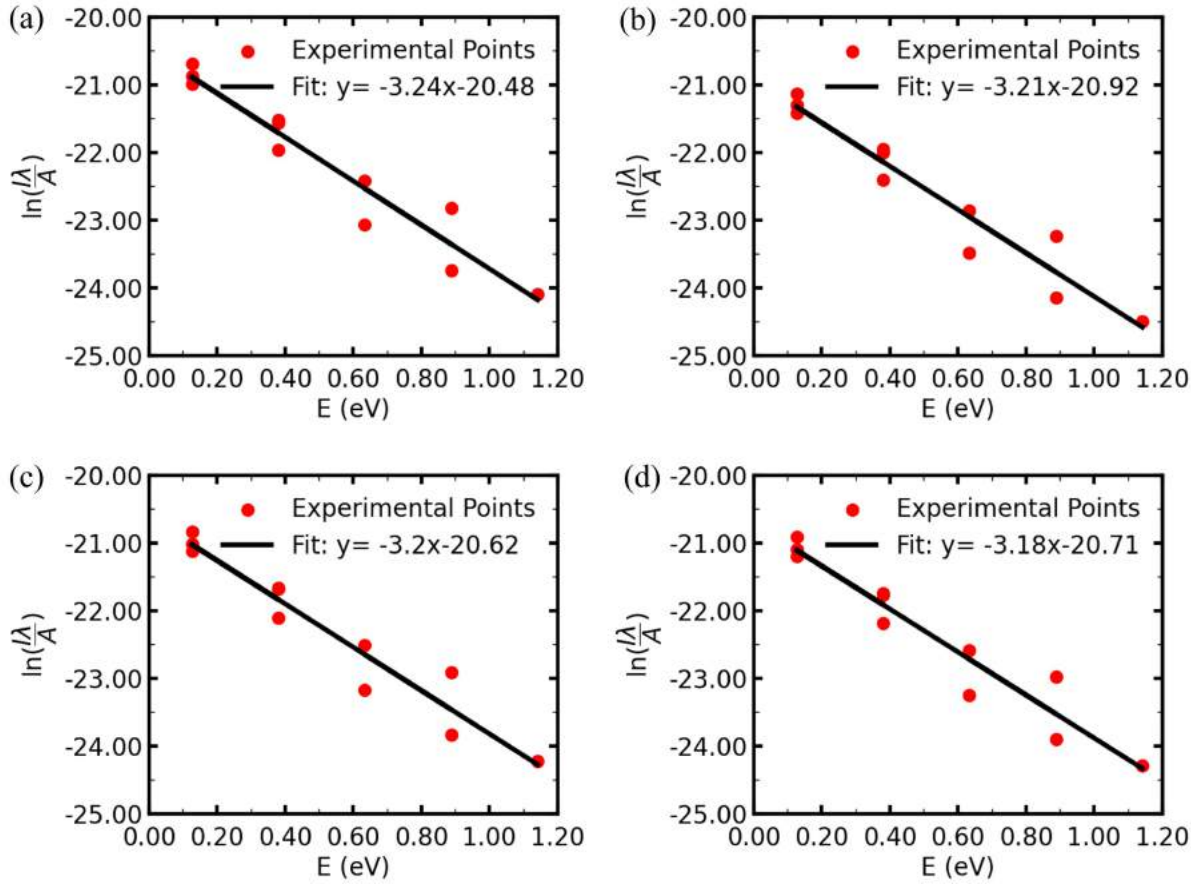

Figure 10: Boltzmann plot for the determination of T_{vib} using nitrogen second positive system N_2 $C^3\Pi_u - B^3\Pi_g$) for flow variation for (a) 0 LPM, (b) 5 LPM, (c) 10 LPM and (d) 15 LPM.

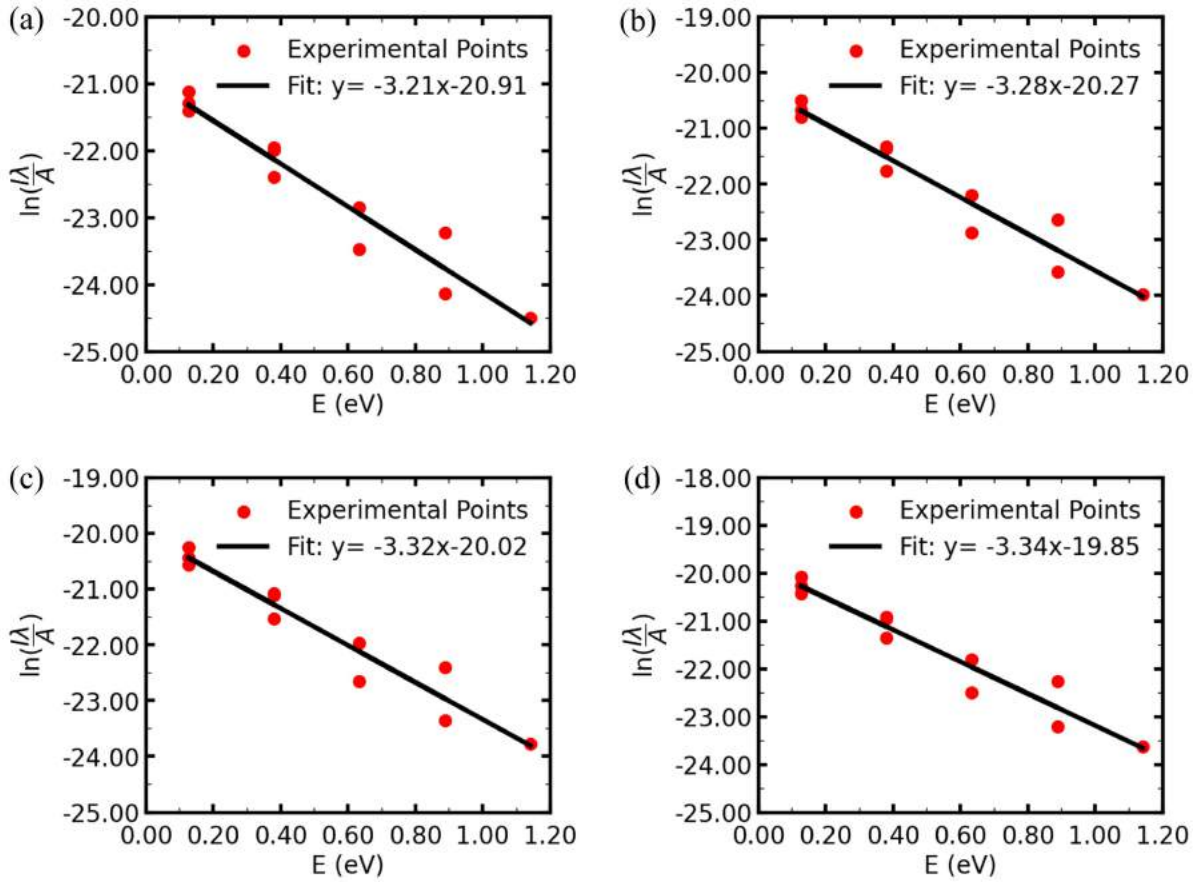

Figure 11: Boltzmann plot for the determination of T_{vib} using nitrogen second positive system N_2 $C^3\Pi_u - B^3\Pi_g$) for increasing applied voltage (a) 12.00 V, (b) 16.00 V, (c) 20.00 V and (d) 24.00 V.

Table 5 shows the optical parameters of APCDBD for increasing air flows at 24.00 V input voltage. As an increase in the airflow electron excitation temperature, and rotational temperature were increased, but density and vibrational temperature decreased. The plasma density decreased with increasing air flow rate is supported by previously published results [63]. Table 6 shows the optical parameters of APCDBD at different input voltages at 15 LPM airflow. While increasing the input voltages of the power supply electron excitation temperature, electron density, vibrational temperature, and rotational temperature are increased. The gas breakdown between the HV electrode and the floating electrode is more likely to occur as the applied voltage increases because of the HV electrode's extremely tiny radius of curvature and the gap, which together produce a strong electric field. Following the disruption in the discharge region, the electron density rises and the plasma resistance value is very low [42]. The plasma power grows with applied voltage, and the energy input into the discharge zone rises as well, increasing the likelihood of electron-heavy particle collisions raising the rotational temperature, and highlighting the Joule heating effect [68].

Table 5: Optical parameters of APCDBD for various air flows at 24.00 V input voltage.

LPM	T_{exc} (K)	N_{e} ($\times 10^{23}$ m^{-3})	$T_{\text{vib(B.P)}}$ (K)	$T_{\text{rot(MOES)}}$ (K)	$T_{vib(MOES)}$ (K)
0	15272.40	1.39	3260.87	492.51 ± 15.13	2759.99 ± 17.59
5	15226.10	1.45	3284.08	486.17 ± 17.95	2762.64 ± 18.19
10	15248.80	1.49	3307.29	474.78 ± 15.93	2777.78 ± 18.35
15	15240.90	1.54	3349.27	464.84 ± 13.56	2787.04 ± 17.85

Table 6: Optical parameters of APCDBD at different input voltage at 15 LPM airflow .

V_{in} (V)	T_{exc} (K)	N_e ($\times 10^{23}$ m^{-3})	$T_{vib(B.P)}$ (K)	$T_{rot(MOES)}$ (K)	$T_{vib(MOES)}$ (K)
12.00	15241.50	1.52	3149.27	450.35 ± 16.23	2743.46 ± 18.57
16.00	15279.10	1.51	3214.45	468.44 ± 16.59	2753.47 ± 18.79
20.00	15293.60	1.53	3291.24	486.01 ± 17.75	2754.24 ± 18.99
24.00	15342.80	1.54	3337.66	496.67 ± 16.49	2787.27 ± 17.85

We have calculated all of the plasma parameters electrical and optical by available analysis techniques in a standard way. We have found our rotational temperature is a little bit more than the room temperature, however, it is decreasing lower but only airflow cannot control the temperature. For this decrement in gas temperature plasma power source is important so we need to develop a power source for reactors for developing heat-sensitive plasma applications. Another major thing of that such types of flat area DBD can treat thin and large surface subtracted but not possible to treat thick substrates. Hence for this application, needed to change such DBD like a plasma jet.

4 Conclusion

In this research, comprehensive electrical and optical characterization of the atmospheric pressure dielectric barrier discharge plasma is employed by available different methods. To understand these basic parameters calculation is essential for every application of plasma. The DBD is produced in atmospheric pressure air so that easy to handle and low cost for production. The energy and power calculation is more converged by using the Lissajous plot method. However, the time-averaged method has more divergent values per cycle. As the airflow increases the energy and power of discharge dissipated also goes on decreasing. Similarly, as the voltage increases the power also increases concerning the parameter. The optical parameters are increased with increasing the input voltage of the power supply, however, density and rotational temperature are decreased while increasing the airflow between the electrodes of APCDBD. It also follows the standard relation of nonthermal plasma temperature order $T_{rot} < T_{vib} < T_{exc}$. The plasma is in a state known as a non-thermal equilibrium when the temperatures of the electrons, vibrations, and rotations are not equal. The rotational temperature, which is assumed to be equivalent to the gas temperature, rises as the applied voltage increases and falls as the airflow increases, suggesting that the thermal effect is more pronounced at higher input voltages and lower airflow. This research work has played a crucial role in understanding the electrical and optical characterization of produced atmospheric discharges.

Acknowledgement

Roshan Chalise would like to acknowledge the University Grants Commission, Nepal for the Ph.D. fellowship award (PhD-78/79-S & T-16) and extend special thanks to Dr. Bhagirath Ghimire for his guidance in the characterization methods. We acknowledge the Research Coordination and Development Council, Tribhuvan University, Kirtipur, Nepal for the National Priority Research Grant (TU-NPAR-077/78-ERG-12). We also thank Tirtha Raj Acharya, Prajwal Lamichhane, and Oat Bahadur Dhakal of Plasma Bioscience Research Center, Department of Electrical and Biological Physics, Kwangwoon University, Seoul, Republic of Korea for their help in determining the vibrational temperature of discharge by Boltzmann plot method.

References

[1] DP Subedi, RB Tyata, R Shrestha, and CS Wong. An experimental study of atmospheric pressure dielectric barrier discharge (DBD) in argon. In *AIP Conference Proceedings*, volume 1588, page 103. American Institute of Physics, 2014. DOI: https://doi.org/10.1063/1.4867673.

[2] Rajesh Prakash Guragain, Hom Bahadur Baniya, Santosh Dhungana, Ganesh Kuwar Chhetri, Binita Sedhai, Niroj Basnet, Aavash Shakya, Bishnu Prasad Pandey, Suman Prakash Pradhan, Ujjwal Man Joshi, et al. Effect of plasma treatment on the seed germination and seedling growth of radish (*Raphanus sativus*). *Plasma Science and Technology*, 24:015502, 2021. DOI: https://doi.org/10.1088/2058-6272/ac3476.

[3] Pradeep Lamichhane, Tirtha Raj Acharya, Neha Kaushik, Linh N Nguyen, Jun Sup Lim, Volker Hessel, Nagendra Kumar Kaushik, and Eun Ha Choi. Non-thermal argon plasma jets of various lengths for selective reactive oxygen and nitrogen species production. *Journal of Environmental Chemical Engineering*, 10:107782, 2022. DOI: https://doi.org/10.1016/j.jece.2022.107782.

[4] LN Mishra, R Dahal, and R Chalise. Impact of plasma treatment on coriander seeds

for germination and growth. *Patan Pragya*, 10:86, 2022. DOI: https://doi.org/10.3126/pragya.v10i01.50598.

[5] Roshan Chalise, Prabin Bhandari, Sangat Sharma, Suresh Basnet, Deepak Prasad Subedi, and Raju Khanal. Enhancement of wheat yield by atmospheric pressure plasma treatment. *AIP Advances*, 13:065104, 2023. DOI: https://doi.org/10.1063/5.0156552.

[6] Roshan Chalise, Pooja Shrestha, Sangat Sharma, Suresh Basnet, Lekha Nath Mishra, and Raju Khanal. Enhancing seed germination and growth parameters of cauliflower *(Brassica oleracea*, variety *botrytis)* using plasma-activated water. *Journal of Physics D: Applied Physics*, 56:505201, 2023. DOI: https://doi.org/10.1088/1361-6463/acf588.

[7] Anil Pudasaini, Dinesh Kumar Chaudhary, Roshan Chalise, Pitamber Shrestha, Leela Pradhan Joshi, and Raju Khanal. Effect of atmospheric dielectric barrier discharge on optical, electrical and surface properties of ZnO film. *Advanced Materials Research*, 1176:43, 2023. DOI: https://doi.org/10.4028/p-w246q7.

[8] Roshan Chalise, Ashish Dahal, Suresh Basnet, Sangat Sharma, Deepak Raj Pant, and Raju Khanal. Effect of plasma-activated water on chlorophyll retention in detached Tejpat *(Cinnamomum tamala)* leaves. *Heliyon*, 10:e24480, 2024. DOI: https://doi.org/10.1016/j.heliyon.2024.e24480.

[9] Ulrich Kogelschatz. Dielectric-barrier discharges: Their history, discharge physics, and industrial applications. *Plasma Chemistry and Plasma Processing*, 23:1, 2003.

[10] H-E Wagner, R Brandenburg, KV Kozlov, A Sonnenfeld, P Michel, and JF Behnke. The barrier discharge: Basic properties and applications to surface treatment. *Vacuum*, 71:417, 2003. DOI: https://doi.org/10.1016/S0042-207X(02)00765-0.

[11] Oat Bahadur Dhakal, Roshani Dahal, Tirtha Raj Acharya, Prajwal Lamichhane, Sandhya Gautam, Bhupendra Lama, Nagendra Kumar Kaushik, Eun Ha Choi, Roshan Chalise, et al. Effects of spark dielectric barrier discharge plasma on water sterilization and seed germination. *Current Applied Physics*, 50:49, 2023. DOI: https://doi.org/10.1016/j.cap.2023.08.006.

[12] Friederike Kogelheide, Björn Offerhaus, Nikita Bibinov, Philip Krajinski, Lars Schücke, Julian Schulze, Katharina Stapelmann, and Peter Awakowicz. Characterisation of volume and surface dielectric barrier discharges in N_2-O_2 mixtures using optical emission spectroscopy. *Plasma Processes and Polymers*, 17:1900126, 2020. DOI: https://doi.org/10.1002/ppap.201900126.

[13] XinPei Lu and Mounir Laroussi. Atmospheric pressure glow discharge in air using a water electrode. *IEEE Transactions on Plasma Science*, 33:272, 2005. DOI: https://doi.org/10.1109/TPS.2005.844946.

[14] Tirtha Raj Acharya, Prajwal Lamichhane, Apurva Jaiswal, Kirubel Amsalu, Young June Hong, Neha Kaushik, Nagendra Kumar Kaushik, and Eun Ha Choi. The potential of multicylindrical dielectric barrier discharge plasma for diesel-contaminated soil remediation and biocompatibility assessment. *Environmental Research*, 240:117398, 2024. DOI: https://doi.org/10.1016/j.envres.2023.117398.

[15] Z Fang, J Lin, X Xie, Y Qiu, and E Kuffel. Experimental study on the transition of the discharge modes in air dielectric barrier discharge. *Journal of Physics D: Applied Physics*, 42:085203, 2009. DOI: https://doi.org/10.1088/0022-3727/42/8/085203.

[16] Annemie Bogaerts, Erik Neyts, Renaat Gijbels, and Joost Van der Mullen. Gas discharge plasmas and their applications. *Spectrochimica Acta Part B: Atomic Spectroscopy*, 57(4):609, 2002. DOI: https://doi.org/10.1016/S0584-8547(01)00406-2.

[17] Jean-Paul Booth, Miran Mozetič, Anton Nikiforov, and Christian Oehr. Foundations of plasma surface functionalization of polymers for industrial and biological applications. *Plasma Sources Science and Technology*, 31(10):103001, 2022. DOI: https://doi.org/10.1088/1361-6595/ac70f9.

[18] Zdeněk Navrátil, Ronny Brandenburg, David Trunec, Antonín Brablec, P St'ahel, Hans-Erich Wagner, and Zdeněk Kopecký. Comparative study of diffuse barrier discharges in neon and helium. *Plasma Sources Science and Technology*, 15:8, 2005. DOI: https://doi.org/10.1088/0963-0252/15/1/002.

[19] Tao Shao, Guangsheng Sun, Ping Yan, and Shichang Zhang. Breakdown phenomena in nitrogen due to repetitive nanosecond-pulses. *IEEE Transactions on Dielectrics and Electrical Insulation*, 14:813, 2007. DOI: https://doi.org/10.1109/TDEI.2007.4286511.

[20] J Reece Roth, Sirous Nourgostar, and Truman A Bonds. The one atmosphere uniform glow discharge plasma (OAUGDP)—A platform technology for the 21^{st} century. *IEEE Transactions on Plasma Science*, 35:233, 2007. DOI: https://doi.org/10.1109/TPS.2007.892711.

[21] Andrey Starikovskiy, Kristofer Meehan, Nikita Persikov, and Richard Miles. Static and dynamic stall control by NS SDBD actuators. *Plasma Sources Science and Technology*, 28:054001, 2019. DOI: https://doi.org/10.1088/1361-6595/ab1461.

[22] G Neretti, AC Ricchiuto, and CA Borghi. Measurement of the charge distribution deposited by an annular plasma synthetic jet actuator over a target surface. *Journal of Physics D: Applied Physics*, 51:324004, 2018. DOI: https://doi.org/10.1088/1361-6463/aacfcb.

[23] Kefeng Shang, Meiwei Wang, Bangfa Peng, Jie Li, Na Lu, Nan Jiang, and Yan Wu. Characterization of a novel volume-surface DBD reactor: discharge characteristics, ozone production and benzene degradation. *Journal of Physics D: Applied Physics*, 53:065201, 2019. DOI: https://doi.org/10.1088/1361-6463/ab538d.

[24] Bangdou Huang, Cheng Zhang, Han Bai, Shuai Zhang, Kostya Ken Ostrikov, and Tao Shao. Energy pooling mechanism for catalyst-free methane activation in nanosecond pulsed non-thermal plasmas. *Chemical Engineering Journal*, 396:125185, 2020. DOI: https://doi.org/10.1016/j.cej.2020.125185.

[25] Changquan Wang, Guixin Zhang, and Xiangning He. Effect of dielectric barrier discharge on semiconductor Si electrode surface. *Applied Surface Science*, 256:6047, 2010. DOI: https://doi.org/10.1016/j.apsusc.2010.03.117.

[26] J Mahoney, W Zhu, VS Johnson, KH Becker, and JL Lopez. Electrical and optical emission measurements of a capillary dielectric barrier discharge. *The European Physical Journal D*, 60:441, 2010. DOI: https://doi.org/10.1140/epjd/e2010-00236-y.

[27] Ying Zhang, Jie Li, Nan Jiang, Ke-Feng Shang, Na Lu, and Yan Wu. Optical characteristics of the filamentary and diffuse modes in surface dielectric barrier discharge. *Spectrochimica Acta Part A: Molecular and Biomolecular Spectroscopy*, 168:230, 2016. DOI: https://doi.org/10.1016/j.saa.2016.05.043.

[28] Zhi Fang, Tao Shao, Shengchang Ji, Jun Pan, and Cheng Zhang. Generation of homogeneous atmospheric-pressure dielectric barrier discharge in a large-gap argon gas. *IEEE Transactions on Plasma Science*, 40:1884, 2012. DOI: https://doi.org/10.1109/TPS.2012.2196029.

[29] Z Fang, Y Qiu, C Zhang, and E Kuffel. Factors influencing the existence of the homogeneous dielectric barrier discharge in air at atmospheric pressure. *Journal of Physics D: Applied Physics*, 40:1401, 2007. DOI: https://doi.org/10.1088/0022-3727/40/5/013.

[30] AP Napartovich. Overview of atmospheric pressure discharges producing nonthermal plasma. *Plasmas and Polymers*, 6:1, 2001. DOI: https://doi.org/10.1023/A:1011313322430.

[31] Richard Engeln, Bart Klarenaar, and Olivier Guaitella. Foundations of optical diagnostics in low-temperature plasmas. *Plasma Sources Science and Technology*, 29:063001, 2020. DOI: https://doi.org/10.1088/1361-6595/ab6880.

[32] Nicolas Balcon, Ana Aanesland, and Rod Boswell. Pulsed RF discharges, glow, and filamentary mode at atmospheric pressure in argon. *Plasma Sources Science and Technology*, 16(2):217, 2007. DOI: https://doi.org/10.1088/0963-0252/16/2/002.

[33] Noriyasu Ohno, M Abdur Razzak, Hiroshi Ukai, Shuichi Takamura, and Yoshihiko Uesugi. Validity of electron temperature measurement by using Boltzmann plot method in radio frequency inductive discharge in the atmospheric pressure range. *Plasma and Fusion Research*, 1:28, 2006. DOI: https://doi.org/10.1585/pfr.1.028.

[34] Nima Pourali, Khuetian Lai, Joe Gregory, Yuyan Gong, Volker Hessel, and Evgeny V Rebrov. Study of plasma parameters and gas heating in the voltage range of nondischarge to full-discharge in a methane-fed dielectric barrier discharge. *Plasma Processes and Polymers*, 20(1):2200086, 2023. DOI: https://doi.org/10.1002/ppap.202200086 publisher=Wiley Online Library.

[35] Nicolas Benard and Eric Moreau. Electrical and mechanical characteristics of surface AC dielectric barrier discharge plasma actuators applied to airflow control. *Experiments in Fluids*, 55:1, 2014. DOI: https://doi.org/10.1007/s00348-014-1846-x.

[36] TC Manley. The electric characteristics of the ozonator discharge. *Transactions of the Electrochemical society*, 84:83, 1943. DOI: https://doi.org/10.1149/1.3071556.

[37] Jerome Pons, Eric Moreau, and Gérard Touchard. Asymmetric surface dielectric barrier discharge in air at atmospheric pressure: Electrical properties and induced airflow characteristics. *Journal of Physics D: Applied Physics*, 38:3635, 2005. DOI: https://doi.org/10.1088/0022-3727/38/19/012.

[38] Shuai Huang, Tie Li, Zhifei Zhang, and Pengfei Ma. Rotational and vibrational temperatures in the spark plasma by various discharge energies and strategies. *Applied Energy*, 251:113358, 2019. DOI: https://doi.org/10.1016/j.apenergy.2019.113358.

[39] Takeshi Sakamoto, Haruaki Matsuura, and Hiroshi Akatsuka. Spectroscopic study on the vibrational populations of $N_2C^3\Pi$ and $B^3\Pi$ states in a microwave nitrogen discharge. *Journal of Applied Physics*, 101:023307, 2007. DOI: https://doi.org/10.1063/1.2426975.

[40] Brett A Cruden, MVVS Rao, Surendra P Sharma, Meyyappan, and M. Neutral gas temperature estimates in an inductively coupled CF_4 plasma by fitting diatomic emission spectra. *Journal of Applied Physics*, 91:8955, 2002. DOI: https://doi.org/10.1063/1.1474614.

[41] Sanghoo Park, Wonho Choe, and Cheorun Jo. Interplay among ozone and nitrogen oxides in air plasmas: Rapid change in plasma chemistry. *Chemical Engineering Journal*, 352:1014, 2018. DOI: https://doi.org/10.1016/j.cej.2018.07.039.

[42] Min Zhang, LIU Yunhu, LI Yao, LI Shuqi, YUAN Hao, Jianping Liang, ZHOU Xiongfeng, and YANG Dezheng. Generation of atmospheric pressure air diffuse discharge plasma in oxygen enriched working gas with floating electrode. *Plasma Science and Technology*, 25:045405, 2023. DOI: https://doi.org/10.1088/2058-6272/aca5f3.

[43] Se Youn Moon, Wonho Choe, Han S Uhm, YS Hwang, and JJ Choi. Characteristics of an atmospheric microwave-induced plasma generated in ambient air by an argon discharge excited in an open-ended dielectric discharge tube. *Physics of Plasmas*, 9:4045, 2002. DOI: https://doi.org/10.1063/1.1495872.

[44] Hoyong Park and Wonho Choe. Parametric study on excitation temperature and electron temperature in low pressure plasmas. *Current Applied Physics*, 10:1456, 2010. DOI: https://doi.org/10.1016/j.cap.2010.05.013.

[45] VA Godyak, RB Piejak, and BM Alexandrovich. Measurement of electron energy distribution in low-pressure RF discharges. *Plasma Sources Science and Technology*, 1:36, 1992. DOI: https://doi.org/10.1088/0963-0252/1/1/006.

[46] Tobias Völker and Igor B Gornushkin. Importance of physical units in the Boltzmann plot method. *Journal of Analytical Atomic Spectrometry*, 37:1972, 2022. DOI: https://doi.org/10.1039/D2JA00241H.

[47] A. Kramida, Yu. Ralchenko, J. Reader, and and NIST ASD Team. NIST Atomic Spectra Database (ver. 5.11), [Online]. Available: https://physics.nist.gov/asd [2024, January 19]. National Institute of Standards and Technology, Gaithersburg, MD., 2023. DOI: https://doi.org/10.18434/T4W30F.

[48] Carlos Aragón and Jose Antonio Aguilera. Characterization of laser induced plasmas by optical emission spectroscopy: A review of experiments and methods. *Spectrochimica Acta Part B: Atomic Spectroscopy*, 63:893, 2008. DOI: https://doi.org/10.1016/j.sab.2008.05.010.

[49] V. K. Unnikrishnan, Kamlesh Alti, V. B. Kartha, C Santhosh, G. P. Gupta, and B. M. Suri. Measurements of plasma temperature and electron density in laser-induced copper plasma by time-resolved spectroscopy of neutral atom and ion emissions. *Pramana*, 74:983, 2010. DOI: https://doi.org/10.1007/s12043-010-0089-5.

[50] Jan Voráč, Petr Synek, Lucia Potočňáková, Jaroslav Hnilica, and Vít Kudrle. Batch processing of overlapping molecular spectra as a tool for spatio-temporal diagnostics of power modulated microwave plasma jet. *Plasma Sources Science and Technology*, 26(2):025010, 2017. DOI: https://doi.org/10.1088/1361-6595/aa51f0.

[51] Jan Voráč, Petr Synek, Vojtěch Procházka, and Tomáš Hoder. State-by-state emission spectra fitting for non-equilibrium plasmas: OH spectra of surface barrier discharge at argon/water interface. *Journal of Physics D: Applied Physics*, 50:294002, 2017. DOI: https://doi.org/10.1088/1361-6463/aa7570.

[52] Jan Voráč, Lukáš Kusỳn, and Petr Synek. Deducing rotational quantum-state distributions from overlapping molecular spectra. *Review of*

Scientific Instruments, 90:123102, 2019. DOI: https://doi.org/10.1063/1.5128455.

[53] Costel Biloiu, Xuan Sun, Zane Harvey, and Earl Scime. Determination of rotational and vibrational temperatures of a nitrogen helicon plasma. *Review of Scientific Instruments*, 77:10F117, 2006. DOI: https://doi.org/10.1063/1.2219392.

[54] Ang Jian Wu, Hao Zhang, Xiao Dong Li, Sheng Yong Lu, Chang Ming Du, and Jian Hua Yan. Determination of spectroscopic temperatures and electron density in rotating gliding arc discharge. *IEEE Transactions on Plasma Science*, 43(3):836, 2015. DOI: https://doi.org/10.1109/TPS.2015.2394441.

[55] Prajwal Lamichhane, Tirtha R Acharya, Jae-Woo Park, Kirubel A Amsalu, Byoungchoo Park, and Eun Ha Choi. Surface activation of thin polyvinyl alcohol films by atmospheric pressure plasma jet: Influence of electron temperature. *Plasma Processes and Polymers*, 20:e2300102, 2023. DOI: https://doi.org/10.1002/ppap.202300102.

[56] Alf Lofthus and Paul H Krupenie. The spectrum of molecular nitrogen. *Journal of Physical and Chemical Reference Data*, 6:113, 1977. DOI: https://doi.org/10.1063/1.555546.

[57] Ronny Brandenburg. Dielectric barrier discharges: progress on plasma sources and on the understanding of regimes and single filaments. *Plasma Sources Science and Technology*, 26:053001, 2017. DOI: https://doi.org/10.1088/1361-6595/aa6426.

[58] M Klas, L Moravsky, Š Matejčik, M Zahoran, V Martišovitš, B Radjenović, and M Radmilović-Radjenović. The breakdown voltage characteristics of compressed ambient air micro discharges from direct current to 10.2 MHz. *Plasma Sources Science and Technology*, 26:055023, 2017. DOI: https://doi.org/10.1088/1361-6595/aa674e.

[59] Francoise Massines, Ahmed Rabehi, Philippe Decomps, Rami Ben Gadri, Pierre Ségur, and Christian Mayoux. Experimental and theoretical study of a glow discharge at atmospheric pressure controlled by dielectric barrier. *Journal of Applied Physics*, 83:2950, 1998. DOI: https://doi.org/10.1063/1.367051.

[60] L Mangolini, K Orlov, U Kortshagen, J Heberlein, and U Kogelschatz. Radial structure of a low-frequency atmospheric-pressure glow discharge in helium. *Applied Physics Letters*, 80:1722, 2002. DOI: https://doi.org/10.1063/1.1458684.

[61] Zhihui Fan, Haicheng Qi, Yidi Liu, Huijie Yan, and Chunsheng Ren. Effects of airflow on the distribution of filaments in atmospheric AC dielectric barrier discharge. *Physics of Plasmas*, 23:123520, 2016. DOI: https://doi.org/10.1063/1.4972095.

[62] N Osawa and Y Yoshioka. Basic processes in fully and partially ionized plasmas-generation of low-frequency homogeneous dielectric barrier discharge at atmospheric pressure. *IEEE Transactions on Plasma Science*, 40:2, 2012. DOI: https://doi.org/10.1109/TPS.2011.2172634.

[63] Soo Hyeon Kim, Jiwon Seo, Yongcheol Hong, Yongwook Shin, Hea-Jong Chung, Ha-Rim An, ChangYeon Kim, Ji-In Park, and Hyun Uk Lee. Construction of an underwater plasma and fenton hybrid system for the rapid oxidation of organic dyes and antibiotics. *Journal of Water Process Engineering*, 52:103519, 2023. DOI: https://doi.org/10.1016/j.jwpe.2023.103519.

[64] NC Roy and MR Talukder. Effect of pressure on the properties and species production in gliding arc Ar, O_2, and air discharge plasmas. *Physics of Plasmas*, 25:093502, 2018. DOI: https://doi.org/10.1063/1.5043182.

[65] Peter J Bruggeman, N Sadeghi, DC Schram, and V Linss. Gas temperature determination from rotational lines in non-equilibrium plasmas: A review. *Plasma Sources Science and Technology*, 23:023001, 2014. DOI: https://doi.org/10.1088/0963-0252/23/2/023001.

[66] Alexander Fridman and Lawrence A Kennedy. *Plasma Physics and Engineering*. CRC press, 2004. DOI: https://doi.org/10.1201/9781482293630.

[67] Tian-Liang Zhao, Yong Xu, Yuan-Hong Song, Xiao-Song Li, Jing-Lin Liu, Jin-Bao Liu, and Ai-Min Zhu. Determination of vibrational and rotational temperatures in a gliding arc discharge by using overlapped molecular emission spectra. *Journal of Physics D: Applied Physics*, 46:345201, 2013. DOI: https://doi.org/10.1088/0022-3727/46/34/345201.

[68] Erich E Kunhardt. Generation of large-volume, atmospheric-pressure, nonequilibrium plasmas. *IEEE Transactions on Plasma Science*, 28:189, 2000. DOI: https://doi.org/10.1109/27.842901.